# Power Quality Improvement in a Three-Phase Grid Tied Photovoltaic System Supplying Unbalanced and Nonlinear Loads

C. Khomsi*, M. Bouzid*, K. Jelassi*

* Université de Tunis EL Manar, LSE-ENIT, ENIT-L.S.E, LR 11 ES 15, BP 37, 1002 Tunis, Tunisia

(chirazkhomsi@gmail.com, monia.Bouzid@yahoo.fr, Khaled.jelassi@enit.rnu.tn)

‡ Corresponding Author ; C. Khomsi; Ecole Nationale d'Ingénieurs de Tunis, LR 11 ES 15, BP 37, Laboratoire des Systèmes Electriques 1002 TUNIS, Tunisia, Tel: +216 52 298 219, Fax: +216 71 872 729,chirazkhomsi@gmail.com

*Received: 05.10.2017 Accepted:29.11.2017*

**Abstract-** This paper is focused on the improvement of the current quality at the Point of Common Coupling (PCC) of a three-phase grid connected photovoltaic system supplying unbalanced and nonlinear loads. The photovoltaic (PV) system is composed of a PV generator interfaced to the grid via a DC–DC power stage connected to a grid-tied inverter. Therefore, to improve the grid current quality at the PCC, the PV inverter is performed as a shunt active power filter in addition to its main task which is the injection of the PV generated power. Thus, this paper proposes a novel and efficient algorithm based on the symmetrical component methodology and the FFT to extract the positive sequence current which represents the balanced fundamental load current. This allows obtaining the correct disturbing current introduced by the nonlinear and unbalanced loads. This disturbing current including the reactive power, harmonic and unbalanced currents, is considered as the reference current in the effective control strategy of the PV inverter. Therefore, the good obtained simulated results point out the effectiveness and the reliability of the proposed algorithm to compensate the disturbing current by eliminating the reactive and unbalanced currents and reducing the total harmonic distortion with a fast dynamic response.

**Keywords** Photovoltaic, Point of Common Coupling, Inverter, Grid Current Quality.

**Nomenclature**

| | |
|---|---|
| $D$ | Duty cycle of the boost converter |
| $f$ | Grid frequency |
| $f_{sw}$ | Switching frequency of the PV inverter |
| $i_{dc}^{*}$ | Output of the current PI controller |
| $I_{dc}$ | Magnitude of the current PI controller |
| $i_{dist}^{*}$ | Reference of the compensating current |
| $i_{F}^{*}$ | Reference current of the current loop |
| $I_{Fmax}$ | Maximum inverter output current |
| $\overline{I}_{La}, \overline{I}_{Lb}, \overline{I}_{Lc}$ | Three unbalanced load currents |
| $\overline{I}_{L1}, \overline{I}_{L2}, \overline{I}_{L0}$ | Complex positive, negative and zero sequence load currents |
| $i_{L1}$ | Fundamental load current |
| $I_{L1}$ | Magnitude of the active load current |
| $i_{L-umb}$ | Unbalanced load current |
| $i_{Lh}$ | Harmonic load current |
| $i_{L\_dist}$ | Disturbing current generated by the load |
| $i_{La-1}(t)$ | Fundamental load current of phase a |
| $i_{La-act}$ | Active component of fundamental load current of phase a |
| $i_{La-react}$ | Reactive component of fundamental load current of phase a |
| $L_f$ | Inductance value of the filter L connected between the PV system and the grid. |
| $Q_a$ | PV inverter reactive power |
| $S_n$ | PV inverter nominal apparent power |
| $u_c$ | PV inverter ouput voltage |
| $u_g$ | Instantaneous grid voltage |
| $U_g$ | Root Mean Square (rms) phase voltage at the PCC |
| $V_{dc}$ | Voltage input of the DC-AC inverter |
| $V_d$ | Direct grid voltage component |
| $V_q$ | Quadrature grid voltage component |

| | |
|---|---|
| $v_{ga}$ , $v_{gb}$ , $v_{gc}$ | Three-phase grid voltages |
| $V_{in}$ | Input voltage of the boost converter |
| $V_{out}$ | Output voltage of the boost converter |
| $X_c$ | Reactance value of the inductance connected to the output side of the inverter |
| $\Delta I_{Fmax}$ | Ripple of the rated output current (peak value) of the DC-AC inverter |
| $\delta$ | Phase angle between the inverter voltage and the grid voltage |
| $\theta_1$ | Phase angle of the active load current |

## 1. Introduction

With the intensive worldwide demand of the electrical power as well as the awareness of environmental problems caused by the extensive use of fossil sources, the penetration of renewable energy sources (RES) into the grid is exponentially increased [1, 2]. The photovoltaic (PV) source is one of the RES that offers a promising alternative to generate green energy and overcoming the energy problems in the world, especially in sunlight abundant regions. Nowadays, the PV systems are largely used as connected to the grid. In fact, grid connected PV systems are very useful since they can ensure the supply of the local loads and transfer the surplus PV generated power to the grid [3]. In this case, installation of storage systems is not important. However, in a PV system, the use of different types of inverters and nonlinear loads introduces various disturbances in the grid [4, 5]. These disturbances which are caused essentially by the harmonics and the reactive current, as well as by the current unbalance, produce negative and undesirable effects on the efficiency of the power distribution systems.

In fact, harmonic content in the grid current can generate overheating in the electrical equipment leading to the increase of losses and the insulation degradation. It also creates ripples in the level of the torque introducing vibrations and noises on motors [6, 7]. On the other hand, an excessive reactive power decreases the power factor and consequently, important losses will be produced.

Moreover, the unbalanced current creates additional losses and neutral current. It generates also pulsating torque in electro-mechanical machines. In addition, it can cause transformer failure because of the flux inside the transformer that will be asymmetrical, leading to increase the winding temperature and subsequently the extra core losses [8, 9].

Consequently, the grid current in a Grid Connected Photovoltaic System (GCPVS) must not exceed the limits of the content harmonic and reactive current, as it is recommended by the standards IEEE 1547 (2003), IEEE 61000-3-2 and IEC 61727[10].

Accordingly, to improve the power quality in a GCPVS, various methods are proposed in the literature review. Recently, Active Power Filter (APF) has been the most employed technique that has received a considerable interest to efficiently improve the power quality. APF has been gaining more attention since it overcomes the drawbacks of classical passive filters [2]. Among the used different APF configurations, the Shunt Active Power Filter (SAPF) is particularly applied to improve the current quality [9]. It is also known as Distribution Static Compensator (DSTATCOM) [11, 12].

In the major proposed studies, the PV inverter connected in parallel to the grid can be used to act simultaneously as a SAPF in addition to its main role which is the transfer of the active power [13, 14]. To do this, the PV inverter must be properly controlled to produce a current equal and opposite to the disturbing current composed of the harmonic, reactive and unbalanced currents generated by the nonlinear loads. In this case, the circulation of this disturbing current will be restricted only to the load side of the power system. Thereby, it is necessary to implement an efficient algorithm, able to extract the reference current used in the control scheme of the PV inverter for extracting the disturbing current introduced by the nonlinear loads. Note that the improvement of the grid power quality is directly affected by the accuracy of the employed technique.

According to recent paper surveys, many interesting algorithms are proposed to determine the exact inverse image of the disturbing load current. Among them, Synchronous Reference Frame (SRF) method and the instantaneous power theory (P-Q theory) which are the most widely used. Each method is able to extract the exact image of harmonic and reactive load currents. In the SRF method, the harmonic and reactive load currents are determined by applying the Park's transformation and a high pass filter. On the other hand, in P-Q theory, the harmonic and reactive load currents are extracted using the instantaneous expression of the active and reactive power and high or band pass filters as well as the Clark's transformation. But the SRF method is not able to rebalance the grid current that is affected by connected unbalanced loads contrary to the P-Q method [15].

The Kalman Filter [16] based technique is also used as reference current extraction method. Although, this technique avoids the use of PI controller that regulates the dc link voltage and it reduces the number of sensors resulting in a reliable and cost effective system, it is not suitable for balancing grid current which is affected by unbalanced loads.

In addition, Phase Locked Loop (PLL) based reference current extraction is proposed in [17]. It is aimed to extract positive and negative sequences of selected harmonics. This means that this technique is able to mitigate grid harmonic currents with unbalance compensation. The dynamic response of this PLL technique is studied under unbalanced system. However, this method requires various control parameters for computation.

A number of adaptive algorithms aimed to extract the reference current have also been proposed. These adaptive filtering techniques have gained more attention due to the good transient response that can be provided compared to the other conventional controls. Besides these techniques are easy to be implemented, the control parameters which are depended to the system dynamics are automatically adjusted [18, 19]. These techniques are designed for the estimation of fundamental active and reactive components that constitute the reference grid current. The estimated components are depended on the optimum Weights. Many adaptive methods are used to determine these Weights such as Least Mean Square (LMS) [20], Variable Least Mean Square (VLMS) [21], Least Mean Fourth (LMF) [22], Leaky Least Mean Fourth [23], Combined Least Mean Square-Least Mean Fourth (LMS-LMF) [24], Reweighted Zero-Attracting (RZA) [18] and Variable Forgetting Factor Recursive Least Square (VFFRLS) [25] techniques. Some other adaptive filtering techniques are also suggested. In [19] which present Adaptive Neuro Fuzzy Inference System Least Mean Square (ANFIS-LMS) algorithm for the calculation of the estimated reference current to improve the grid power quality, the LMS technique is used for finding weighted components. This LMS technique depends on the Step Size parameter which is updated from the Neuro Fuzzy Inference System (ANFIS). In this paper, a comparison between the performance ANFIS-LMS, Fixed Step LMS and Variable Step LMS is investigated and demonstrated that the ANFIS-LMS algorithm is better in terms of harmonic compensation and less static error.

A comparison between two Artificial Neural Network (ANN) based technique for reference current extracting is investigated in [26]. The first one is based on Adaptive Linear Neuron (Adaline) algorithm which is trained on line by the LMS algorithm while the second ANN technique uses the Multilayer Neural Network (MNN) which is trained off line using the Scaled Conjugate Gradient (SCG) propagation algorithm. The comparison study between the performances of these two techniques shows that the Adaline based technique control technique has better accuracy in the extraction of the fundamental current.

A Wiener filter based control algorithm is proposed to estimate weights in [27] and compared to LMS algorithm. It has demonstrated that Wiener filter algorithm achieves faster convergence than LMS algorithm under a modified steady state as well as dynamic load condition.

Therefore, although the efficiency of these above mentioned adaptive filtering techniques, they suffer with the drawbacks of time delay and complex calculations

In this paper, an efficient, accurate and simple algorithm is proposed having the originality to compensate reactive, harmonic and unbalanced currents introduced by connected loads in a GCPVS with a fast dynamic response. This technique is based on the use of the Symmetrical Components (SC) in order to determine the balanced active current of the local loads, at the fundamental grid frequency using a PLL technique.

This paper is organized as follows. In section 2, a detailed description of the used GCPVS is presented. Section 3 is aimed to discuss the proposed control scheme of the PV Inverter with a presentation of the proposed method to generate the disturbing load current. The efficiency of this proposed method is demonstrated in section 4 by the good obtained results. In fact, it has been pointed out by simulation, that the proposed algorithm has significantly improved the quality of the grid current by providing a balanced current with a low harmonic content and a good PF. In addition, the proposed method is simple to implement and presents a fast dynamic response and short time computing.

## 2. Description of the Proposed Grid Connected Photovoltaic System (GCPVS)

The global structure of the considered GCPVS is illustrated in Fig.1. It is composed of a PV generator connected to the grid by the intermediate of a boost DC-DC converter which is followed by a DC-AC three phase voltage source inverter. Unbalanced and nonlinear loads are connected at the PCC of the GCPVS.

To reduce the high harmonic current components, an inductive filter L is connected between the PV system and the grid. The selection of the inductance value of this filter directly affects the performance of the APF. The adequate inductance value can be calculated according to (1) [28].

$$L_f = \frac{0{,}5.V_{dc} - 0{,}5.\frac{V_{dc}}{2}}{2\Delta I_{Fmax}} \cdot \frac{1}{2f_{sw}} \tag{1}$$

The maximum inverter output current $I_{Fmax}$ is related to the nominal apparent power of the inverter ($S_n$) according to (2).

$$I_{Fmax} = \frac{\sqrt{2}.S_n}{3.U_g} \tag{2}$$

### 2.1. PV Generator

The used PV generator is conceived on Matlab/Simulink as an association of two strings in parallel, where each string is composed of 26 PV modules connected in series, to obtain a PV generator with a rated power of 13kWc at the nominal Standard Test Conditions (STC) of cells temperature T (25°C) and irradiance G (1000W/m2). Fig.2 shows the characteristics of $I_{PV}$ –$V_{PV}$ and $P_{PV}$-$V_{PV}$. The electrical parameters of the PV generator are represented in Table 1.

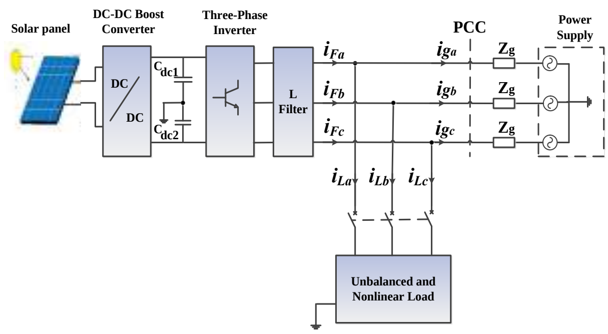


**Fig. 1.** The structure of the used grid tied photovoltaic system

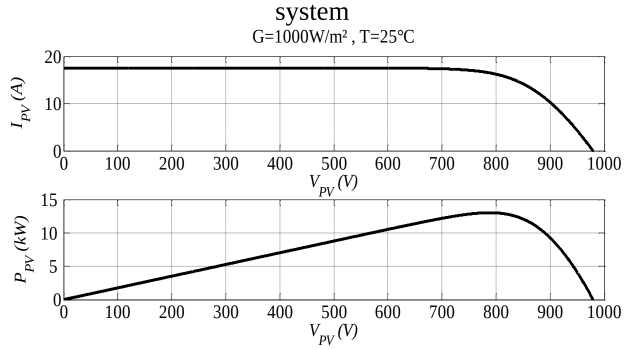


**Fig. 2.** Characteristics $I_{PV}$ –$V_{PV}$ and $P_{PV}$ –$V_{PV}$ of the used PV generator

**Table 1.** Simulated electrical parameters of the used PV module at the STC

| Parameters | Symbols | Values |
|---|---|---|
| Short Circuit Current | $I_{sc}$ (A) | 8.66 |
| Open Circuit Voltage | $V_{sc}$ (V) | 37.88 |
| Voltage at MPP | $V_{mpp}$ (V) | 30.5 |
| Current at MPP | $I_{mpp}$ (A) | 8.24 |
| Power at MPP | $P_{mp}$ (W) | 251W |
| Voltage Temperature | $K_v$(mV/°C) | -0.340 |
| Current Temperature | $K_i$(mA/°C) | 0.049 |
| Number of PV modules | N | 52(2×26) |

### *2.2. DC-DC Boost Converter*

The use of a converter, type boost, is to step up the solar input voltage to a required value of the output voltage. The relation between ($V_{in}$) and ($V_{out}$) is given by (3).

$$V_{out} = \frac{V_{in}}{(1\text{-}D)} \tag{3}$$

The DC-DC boost converter is controlled by the Maximum Power Point Tracking (MPPT) control, to ensure the transfer of the maximum power delivered by the PV generator. It is based on the looking for the closest point to the maximum solar power at each moment. Many MPPT methods are proposed in the literature such as Perturb and Observe (P&O) method, Incremental Conductance (IC) method, Fuzzy Logic method, curve fitting technique and Look Up Table Method. In this paper, the (P&O) method is used to extract the maximum PV power, since P&O is characterized by a good accuracy in getting the real Maximum Power Point (MPP) in a short time with a simple implementation[29, 30] .

## 3. Description of the Proposed Control Scheme of the PV Inverter

The PV system connected to the grid through a three-phase inverter. This inverter has the main task to supply the loads connected at the PCC and transfer the surplus of the PV power to the grid. Therefore, in order to protect the connected loads to the grid, the current at the PCC must be of a high quality, which means that the grid current should be sinusoidal balanced one, with a low THD and reactive current according to the limits recommended by the standard.

Thus, to improve the grid current quality, the PV inverter is performed as a SAPF in addition to its main function which is the injection of the PV power to the grid. In this case, an efficient and reliable control strategy, represented in Fig.3, is applied to the three-phase grid tied inverter. As shown in Fig.3, the control strategy of the PV inverter is based on two cascaded loops. The first loop is the inner fast current loop, that regulates the inverter output current, and the second one is the external DC-voltage control loop.

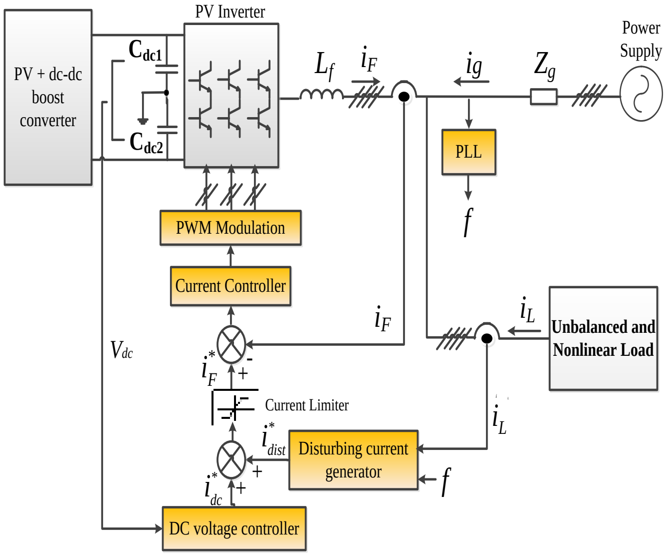


**Fig.3.** A description of the control scheme of the PV inverter of the GCPVS

### *3.1. DC Voltage Control Loop*

The PV inverter must inject the active and reactive power to the electric power system. According to (4) in [28], the reactive power provided by the inverter depends on the magnitude of the fundamental component of the inverter's output voltage ($u_c$).

$$Q_a = \frac{u_g(u_c \cos\delta - u_g)}{X_c} \tag{4}$$

This injected reactive power should ensure the compensation of the load reactive power. To do that, the magnitude of the fundamental component of the inverter's AC voltage ($u_c$) must be higher than the grid voltage amplitude [28]. For this reason, the voltage of the capacitor installed in the DC side of the inverter, that is equal to the AC voltage amplitude of the inverter, must be stabilized and maintained to a value higher than the magnitude of the grid voltage in order to ensure the power flow balancing. On the other hand, a higher DC voltage value can improve the harmonic compensation performance of the inverter [31]. The minimum DC link voltage required is about 2.8 times the grid voltage [32].

In this work, the selected reference voltage $V_{dc}^*$ value is equal to 840 V. Thus, an outer DC-voltage control loop must be implemented. Thanks to this control loop, the DC-bus voltage will be maintained to the desired reference voltage $V_{dc}^*$ .

A Proportional Integrator (PI) controller is used to ensure a zero-steady-state error between the DC-voltage $V_{dc}$ and the desired voltage $V_{dc}^*$ . The output of this employed PI controller is expressed by (5).

$$i_{dc}^* = I_{dc}.\sin(2\pi.f.t) \tag{5}$$

*3.2. Inner Current Control Loop*

The inner current loop consists of comparing the inverter output current $i_F$ to its reference $i_F^*$. The error of this comparison is set to zero using a PI controller so that the PV inverter is forced to produce a current $i_F$ identical to its reference $i_F^*$. The output of the PI controller is the reference voltage of the PWM block to generate the six pulses to control the six inverter switches.

The reference current $i_F^*$, is expressed by (6).

$$i_F^* = i_{dist}^* + i_{dc}^* \tag{6}$$

*3.3. Disturbing Current Generator*

The disturbing current generator is the block that permits to extract the correct disturbing current using an original algorithm depicted in Fig.4. This algorithm is essentially based on the symmetrical component method. With the symmetrical components methodology, any set of unbalanced three-phase current can be transformed into three sets of symmetrical balanced components known as positive $\overline{I}_1$, negative $\overline{I}_2$ and zero $\overline{I}_0$ sequences.

Therefore, based on the symmetrical component method the positive, negative and zero sequences load current in their complex form, obtained from $\overline{I}_{La}$, $\overline{I}_{Lb}$, $\overline{I}_{Lc}$ (see Fig.1), can be calculated using the complex Fortescue's transformation as it is expressed by (7), (8) and (9) [33].

$$\overline{I}_{L1}=\frac{1}{3}(\overline{I}_{La}+\overline{a}.\overline{I}_{Lb}+\overline{a}^2.\overline{I}_{Lc}) \tag{7}$$

$$\overline{I}_{L2}=\frac{1}{3}(\overline{I}_{La}+\overline{a}^2.\overline{I}_{Lb}+\overline{a}.\overline{I}_{Lc}) \tag{8}$$

$$\overline{I}_{L0}=\frac{1}{3}(\overline{I}_{La}+\overline{I}_{Lb}+\overline{I}_{Lc}) \tag{9}$$

Where $\overline{a}=e^{j\frac{2\pi}{3}}$ and $\overline{a}^2=e^{j\frac{4\pi}{3}}$

Therefore, based on Fig.4, the principle of the proposed algorithm consists of determining the active balanced load current at the fundamental grid frequency, to subtract it from the total unbalanced load current. Thus, the obtained current is the disturbing one which is composed of the harmonic, reactive and unbalanced currents.

To obtain the active balanced current, first, the magnitude $I$ and the phase angle $\theta_{iL}$ of each load current $i_L$ are determined by applying the Fast Fourier Transformation (FFT) at the fundamental frequency of the grid, using a PLL describes later. These magnitudes and phase angles are then used to calculate the complex Positive Sequence Current (PSC) $\overline{I}_{L1}$ expressed by (7). Note that the PSC is the fundamental component of the balanced three-phase load current.

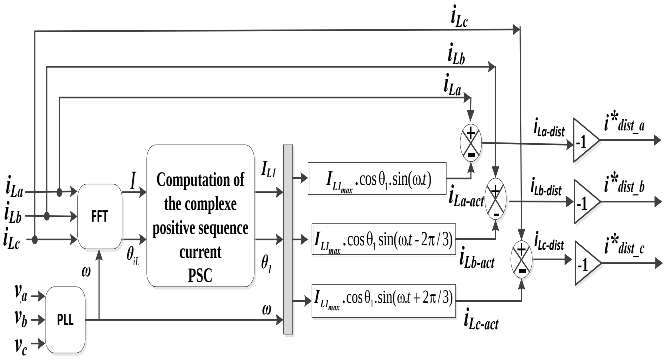


**Fig. 4.** Disturbing current generation block

Subsequently, the magnitude and phase angle of the complex PSC are extracted to determine the active load current. Once the active load current is obtained, it is subtracted from the total three-phase load current in order to isolate the accurate disturbing current as illustrated in Fig.4.

The proposed algorithm can be demonstrated mathematically as follows:

The current of a **balanced** three-phase load can be expressed by (10) and (11).

$$\begin{cases} i_{La}(t)=\sum_{h=1}^{\infty} I_h sin(h\omega t+\theta_h) \\ i_{Lb}(t)=\sum_{h=1}^{\infty} I_h sin(h\omega t+\theta_h-\frac{2\pi}{3}) \\ i_{Lc}(t)=\sum_{h=1}^{\infty} I_h sin(h\omega t+\theta_h+\frac{2\pi}{3}) \end{cases} \tag{10}$$

$$\begin{cases} i_{La}(t)=I_{L1_{max}}.sin(\omega t+\theta_1) + \sum_{h=2}^{\infty} I_h sin(h\omega t+\theta_h) \\ i_{Lb}(t)=I_{L1_{max}}.sin(\omega t+\theta_1-\frac{2\pi}{3})+\sum_{h=2}^{\infty} I_h sin(h\omega t+\theta_h-\frac{2\pi}{3}) \\ i_{Lc}(t)=I_{L1_{max}}.sin(\omega t+\theta_1+\frac{2\pi}{3})+\sum_{h=2}^{\infty} I_h sin(h\omega t+\theta_h+\frac{2\pi}{3}) \end{cases} \tag{11}$$

According to (11), is expressed by (12)

$$i_L(t)=i_{L1}(t)+i_{Lh}(t) \tag{12}$$

However, the fundamental current, can be decomposed of active and reactive components as it is shown by (13), for the case of the load current of the phase "a".

$$\begin{aligned} i_{La\text{-}1}(t)&=I_{L1\text{-}max} sin(\omega t+\theta_1) \\ &=I_{L1\text{-}max}.cos(\theta_1).sin(\omega t)+I_{L1\text{-}max}.sin(\theta_1).cos(\omega t) \\ &=i_{La\text{-}act}(t)+i_{La\text{-}react}(t) \end{aligned} \tag{13}$$

Therefore, to determine the active current, the magnitude $I_{L1}$ and the phase angle $\theta_1$ are calculated from the PSC using the symmetrical component.

Thus, the three-phase active current of the nonlinear load is

$$\begin{cases} i_{La\text{-}act}(t)=I_{L1_{max}}\cos\theta_1.\sin(\omega.t) \\ i_{Lb\text{-}act}(t)=I_{L1_{max}}\cos\theta_1.\sin(\omega.t-\frac{2\pi}{3}) \\ i_{Lc\text{-}act}(t)=I_{L1_{max}}\cos\theta_1.\sin(\omega.t+\frac{2\pi}{3}) \end{cases} \quad (14)$$

Now, for an **unbalanced** three-phase load, the unbalanced current can be expressed by (15).

$$i_L(t)=i_{L\text{-}act}(t)+i_{L\text{-}react}(t)+i_{Lh}(t)+i_{L\text{-}umb}(t) \quad (15)$$

With

The disturbing current is the sum of the reactive, harmonic and unbalanced currents as it is shown by (16).

$$i_{L\_dist}(t)=i_{L\text{-}react}(t)+i_{Lh}(t)+i_{L\text{-}umb}(t) \quad (16)$$

Thus, using (15) and (16), the disturbing current can be obtained by subtracting the active load current from the measured load current.

$$i_{L\text{-}dist}(t)=i_L(t)-i_{L\text{-}act}(t) \quad (17)$$

As it is illustrated in Fig.7, a minus sign is applied to $i_{L\text{-}dist}$ to obtain the opposite of the disturbing current ($-i_{L\text{-}dist}$) taken as the reference compensating current in the current loop of the PV inverter control scheme.

### *3.4. Phase Locked Loop (PLL)*

The PLL has the main function to measure the instantaneous phase angle $\theta$ and the frequency $f$ of the grid voltage. In this paper, the used PLL is based on the Synchronous Reference Frame PLL (SRF-PLL) technique which is described in [34, 35]. Its basic scheme is illustrated in Fig.5, where the three grid voltages are converted to the direct and quadrature grid voltage components into synchronous reference frame by applying the Park's transformation matrix according to equation (18).

$$\begin{bmatrix} V_d \\ V_q \\ V_0 \end{bmatrix} = \frac{2}{3}\begin{bmatrix} \cos(\theta) & \cos(\theta-\frac{2\pi}{3}) & \cos(\theta+\frac{2\pi}{3}) \\ -\sin(\theta) & -\sin(\theta-\frac{2\pi}{3}) & -\sin(\theta+\frac{2\pi}{3}) \\ \frac{1}{2} & \frac{1}{2} & \frac{1}{2} \end{bmatrix} \cdot \begin{bmatrix} v_{ga} \\ v_{gb} \\ v_{gc} \end{bmatrix} \quad (18)$$

The phase angle $\theta$ of the rotating reference frame is obtained from its angular frequency ω. This angular frequency ω is equal to the angular frequency of the grid ($\omega_{grid}$), since the grid voltage is synchronized with the rotating dq axis.

From Fig. 5, to extract the angular frequency ω, the grid voltage quadrature axis $V_q$ is fixed to zero using a PI controller. Therefore, the grid voltage direct axis $V_d$ will be equal to the grid voltage amplitude $V_{gm}$.

The frequency $f$ of the grid voltage is determined by dividing the angular frequency (ω) which is produced in the PI controller output by (2.π).

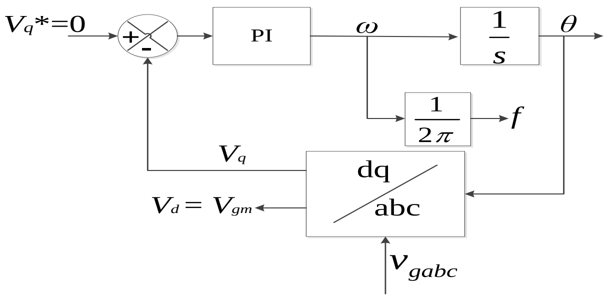


**Fig. 5.** Schematic diagram of the SRF-PLL

## 4. Simulation Results

To evaluate the performance and the efficiency of the control strategy and the proposed algorithm useful to extract the disturbing current, the considered GCPVS of Fig.1, supplying unbalanced and nonlinear loads was implemented in Matlab /Simulink and simulated with a sample step equals to 1µs.

As shown in Fig.6, three loads are connected at the PCC of the GCPVS. The first load $\mathcal{L}_1$ is a nonlinear three-phase one composed by a three-phase full wave rectifier feeding an inductive (RL) load with (R= 61Ω and L=20mH), the second load $\mathcal{L}_2$ is a resistive one ($R_2$) connected at the phase "b" with $R_2$=80Ω, and the third load $\mathcal{L}_3$ is also a resistive one ($R_3$) with $R_3$=35Ω connected at the phase "c".

Before studying the quality of the grid current, it is convenient to analyze first, the total three-phase current of the three connected loads ($\mathcal{L}_1$, $\mathcal{L}_2$, $\mathcal{L}_3$) at the PCC. These three loads consume a total active power of 6930 W. The total current consumed by the three loads is represented in Fig.7. It can be noted that the three load currents $i_{La}$, $i_{Lb}$ and $i_{Lc}$ are unbalanced and highly distorted since they have not the same magnitude and they present a high THD, as indicated in Table 2.

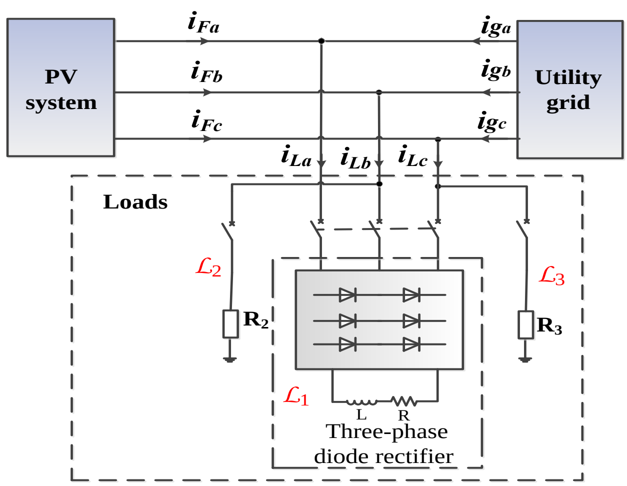


**Fig. 6.** Description of the three used loads connected at the PCC of the GCPVS

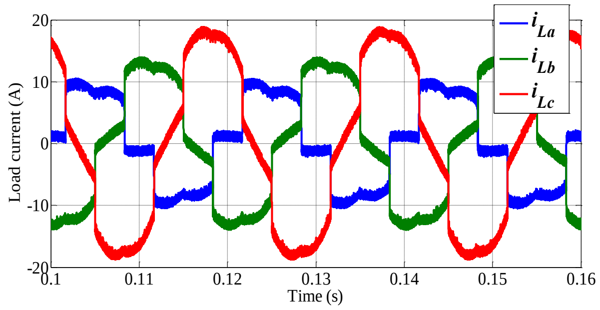


**Fig. 7.** Simulated three-phase load current

**Table 2.** Magnitude and THD values of the three curents of the loads connected at the PCC

| | $i_{La}$ | $i_{Lb}$ | $i_{Lc}$ |
|---|---|---|---|
| **Magnitude (Peak value) (A)** | 9.808 | 13.86 | 19.09 |
| **THD (%)** | 30.13 | 21.4 | 15.49 |

The study of the grid current quality consists to evaluate the efficiency of the proposed method by evaluating the quality of the three grid currents $i_{ga}$, $i_{gb}$ and $i_{gc}$. In fact, in this aim, using the proposed algorithm, the THD index, the PF, the magnitude and the frequency of the grid current must be thoroughly studied. As the delivered PV power depends on the climatic conditions, the quality of the grid current is therefore studied in three different operating modes of the PV system. This study is achieved according to a chosen profile of the PV generator represented in Fig.8. In the first mode (Mode1), the grid current is studied in the case of a total absence of both solar irradiance and temperature (G=0 W/m$^2$ and T=0°C for 0<t<0.4s), where the PV system performs only as a SAPF. In the second (Mode 2) and the third (Mode 3) modes, the quality of the grid current is studied in the case of a presence of the solar irradiance and temperature, where the PV inverter is equipped by the two functionalities: the injection of the PV power and the filtering (SAPF). The solar irradiance and the temperature in case of Mode 2 are equal to 1000W/m$^2$ and 25°C respectively (G=1000W/m$^2$ and T=25°C for 0.4<t<0.8s). While in Mode 3, the solar irradiance and temperature are equal to 200W/m$^2$ and 5°C (G=200W/m$^2$ and T=5°C for 0.8<t<1.2s). For these three modes, the transfer of the active power between the three elements, the PV generator, the grid and the loads, and the waveform of the three-phase grid current are also simulated and illustrated in Figures 9 and 10 respectively.

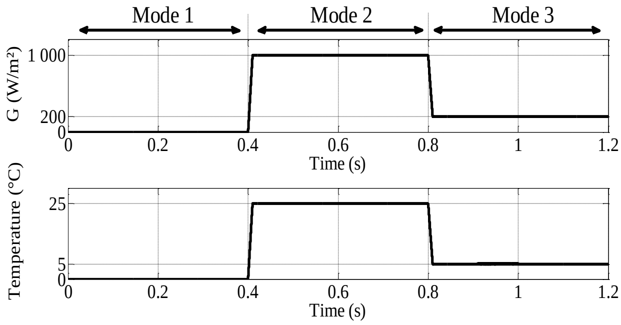


**Fig. 8.** Irradiance and temperature profiles of the PV generator

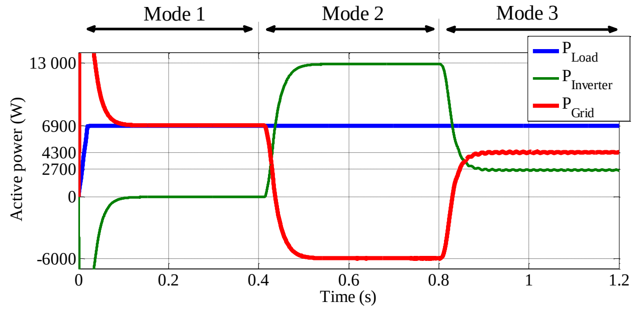


**Fig. 9.** Simulated active power of the load, PV inverter and the grid.

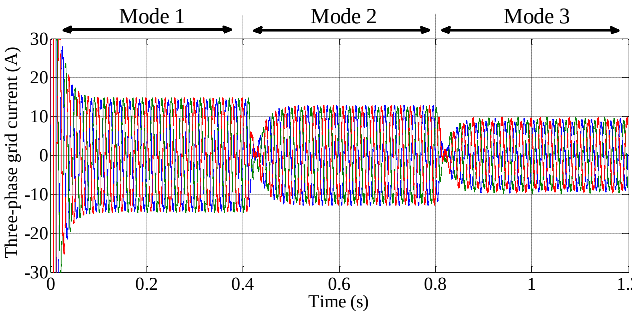


**Fig. 10.** Simulated three-phase grid current in the three operating modes

*4.1. Study of the Grid Current Quality in Mode 1*

This proposed operating mode is obtained when the solar irradiance and temperature are null, as shown in Fig.8 between t= 0s and t=0.4s. In this range, the PV inverter power is null (Ppv=0W). Therefore, the connected loads at the PCC are supplied only by the grid, as it is illustrated in Fig. 9, where the gird active power is equal to the one of the loads. In this mode, the three-phase grid current is represented in Fig.11. To well point out the characteristics of each grid current, the three grid currents $i_{ga}$, $i_{gb}$ and $i_{gc}$ are represented in Figures 12,13, and 14, in frequency domain. As it can be seen, $i_{ga}$, $i_{gb}$ and $i_{gc}$ present a low THD equal to 1.48%, 1.33%, and 1.82% respectively. The three grid currents $i_{ga}$, $i_{gb}$ and $i_{gc}$ have almost the same magnitudes which are equal to 14.1A, 14.34A and 14.22A respectively and they are shifted by 120°. Furthermore, it has been noted that the grid voltage and current are in phase as it is illustrated in Fig.15, which means that the reactive current is null and the PF=1.

Therefore, it can be concluded that in Mode 1, the three grid currents $i_{ga}$, $i_{gb}$ and $i_{gc}$ constitute a balanced sinusoidal three-phase current, with a magnitude of 14.2 A, a frequency of 50 Hz, a low THD level of 1.5%, and a PF=1.

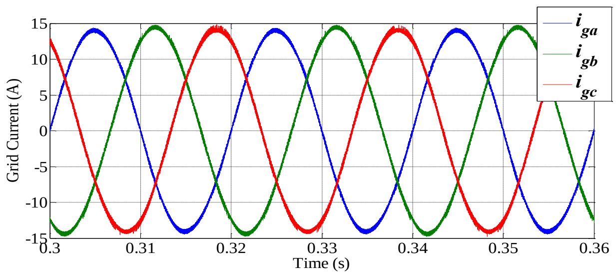


**Fig. 11.** Simulated grid current in Mode 1

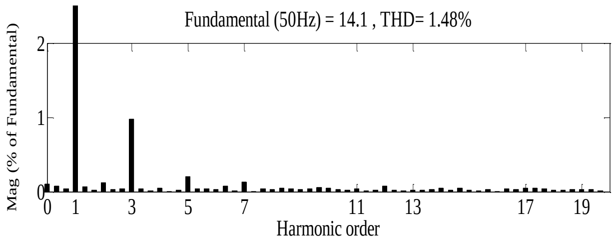


**Fig. 12.** Frequency representation of the current $i_{ga}$ in Mode1

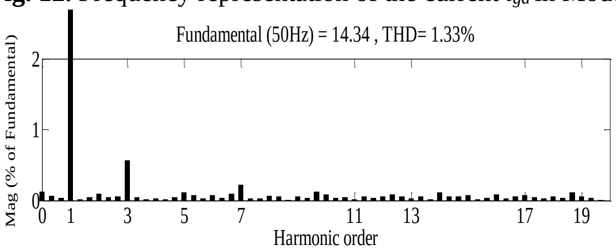


**Fig. 13.** Frequency representation of the current $i_{gb}$ in Mode1

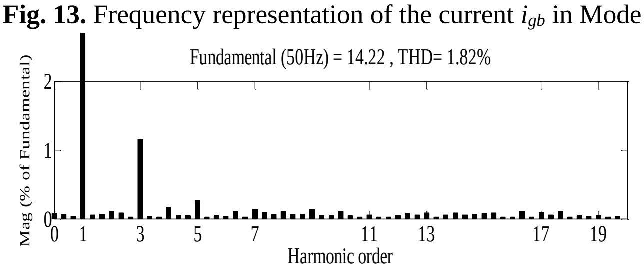


**Fig. 14.** Frequency representation of the current $i_{gc}$ in Mode1

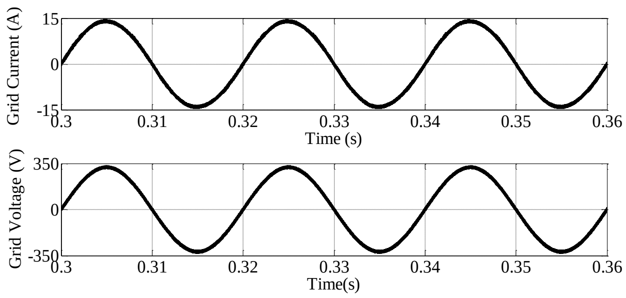


**Fig. 15.** The Shape of the grid voltage and current of phase "a" at the PCC in Mode 1

*4.2. Study of the Grid Current Quality in Mode 2*

In this operating mode the solar irradiance and temperature are set respectively to 1000W/m$^2$ and 25°C as it is shown in Fig.8 for 0.4s <t < 0.8s. In this case, according to Fig.9, the PV inverter power which is equal to 13kW is higher than the load power. Thus, the PV system provides the required power of the loads and the surplus is injected into the grid. In this mode, the three-phase grid current is simulated and represented in Fig.16. The THD and the magnitude of the three grid currents $i_{ga}$, $i_{gb}$ and $i_{gc}$, are shown in Figures 17, 18 and 19 respectively. Accordingly, the THD levels of $i_{ga}$, $i_{gb}$ and $i_{gc}$ are low and equal to 1.82%, 1.77 %, and 2.19% respectively. The magnitudes of $i_{ga}$, $i_{gb}$ and $i_{gc}$ are balanced and equal to 12.42 A, 12.18 A, and 12.29 A respectively, and they are shifted by 120°. In addition, based on Fig.20, it can be noted that the grid voltage ($v_{ga}$) and current ($i_{ga}$) of the phase "a" are in opposite phase, since the current is injected in the grid (the grid behaves as a receptor), and consequently the reactive current is null and the PF is equal to the unit. However, it can be concluded that in Mode 2, the three grid currents form a balanced sinusoidal three-phase current with a magnitude equal almost to 12,3 A, a frequency of 50 Hz, a low THD of almost 1.9% and a PF=1.

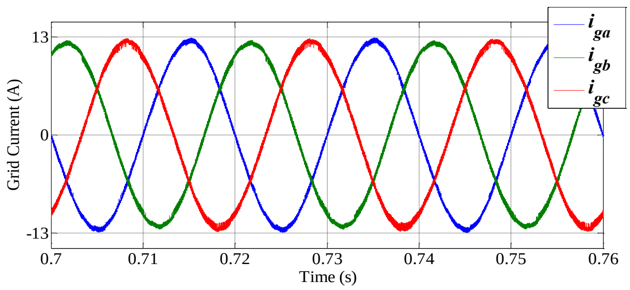


**Fig. 16.** Simulated three-phase grid current in Mode2

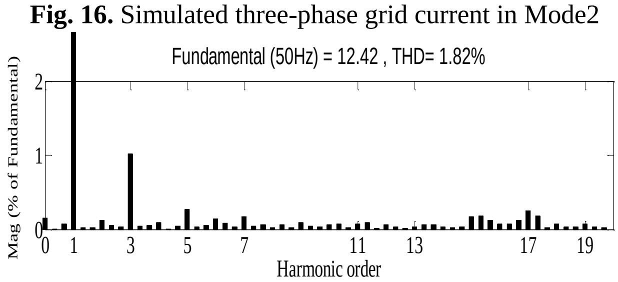


**Fig. 17.** Frequency representation of the current $i_{ga}$ in Mode2

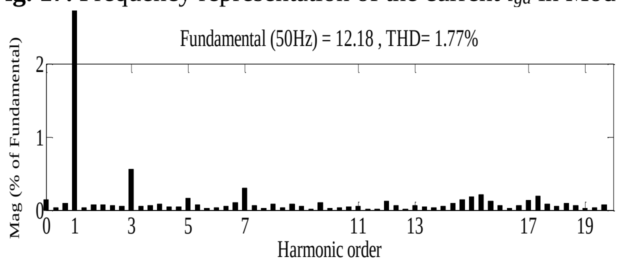


**Fig. 18.** Frequency representation of the current $i_{gb}$ in Mode2

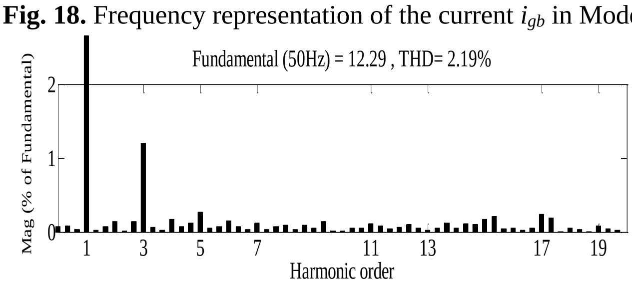


**Fig. 19.** Frequency representation of the current $i_{gc}$ in Mode2

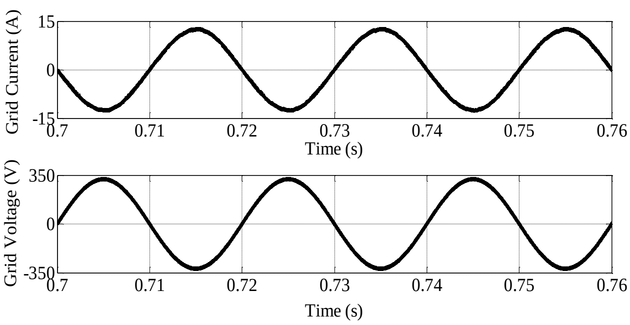


**Fig.20.** The Shape of the grid voltage and current of the phase "a" at the PCC in Mode 2

### *4.3. Study of the Grid Current Quality in Mode 3*

In this operating mode, the solar irradiance and temperature are set respectively to 200W/m$^2$ and 5°C as it is shown in Fig.8 for 0.8s <t < 1.2s. In this case, according to Fig.9, the loads are supplied simultaneously by the PV system and the grid since the active power delivered by the PV generator is equal to 2650 W, less than the necessary required load power. Therefore, to compensate the lack of power from the PV, the loads take their necessary power from both the PV system (2650 W) and the grid (4280 W). In this mode, the three-phase grid current is illustrated in Fig.21. The THD and the magnitude of the three fundamental grid currents $i_{ga}$, $i_{gb}$ and $i_{gc}$ are represented in Figures 22, 23, and 24 respectively. The THD of these three currents are equal to 2.23 %, 2.24 %, and 2.86%, while their magnitudes are equal to 8.749 A, 8.979 A, and 8.871 A respectively. Note that the three currents are shifted by 120°. In addition, according to Fig.25 which represents the waveforms of the grid voltage and current of phase "a", it can be noted that the PF is equal to 1 as the voltage and the current are in phase. Thus, in this mode, the three grid currents form a balanced three-phase sinusoidal current, with a magnitude of almost 8.8 A, a frequency of 50 Hz, a low THD of 2.5% and a PF =1.

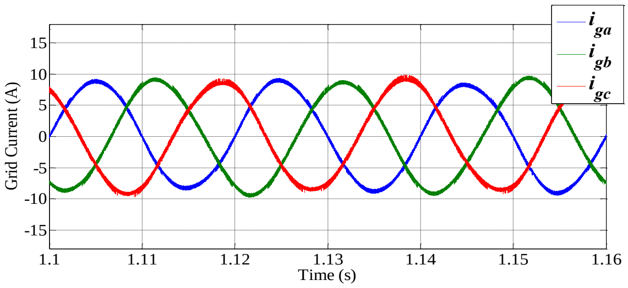


**Fig. 21.** Simulated three-phase grid current in Mode 3

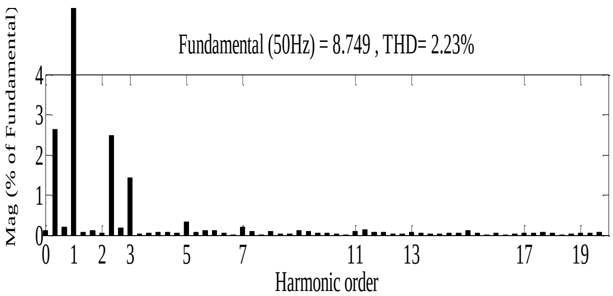


**Fig. 22.** Frequency representation of the current $i_{ga}$ in Mode3

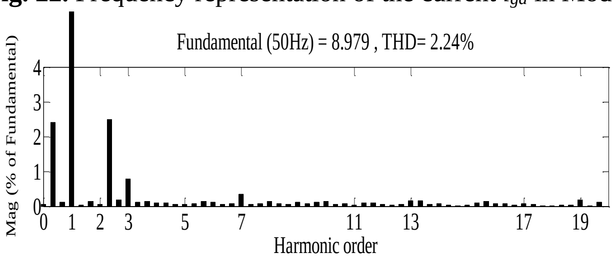


**Fig. 23.** Frequency representation of the current $i_{gb}$ in Mode3

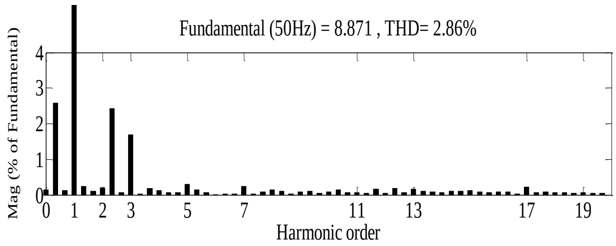


**Fig. 24.** Frequency representation of the current $i_{gc}$ in Mode3

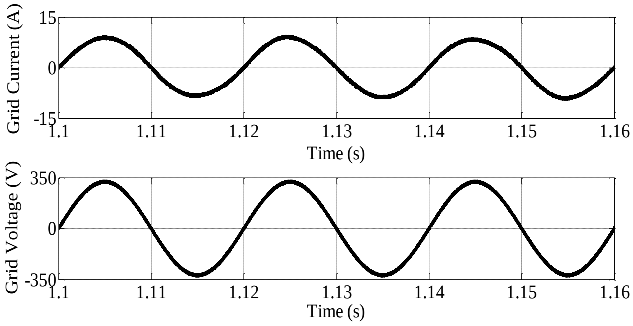


**Fig. 25.** The shape of the grid voltage and current of the phase "a" at the PCC in Mode 3

### *4.4. Recapitulation of the Grid Current Quality in the three modes*

The obtained results in the above study in the three modes of the PV system are recapitulated in Table 3. Therefore, according to these results, it can conclude that with the proposed algorithm for the extraction of the correct disturbing current, the GCPVS performs with a high quality of the grid current at the PCC, in any operating point of the PV system since:

- The three grid currents have sinusoidal waveforms with a low value of THD, ranged between 1.3% and 2.8% in the three modes, as shown in Table 3.

- The three grid currents are well balanced. They have almost the same magnitude (Table 3) and they are shifted by 120°, under any operating point of the PV system. In addition, as it is illustrated in Fig.26, the neutral current is null in the three modes which proves that the grid current is balanced.

- The grid current does not present a reactive component in the three modes as it is represented in Fig.27. Therefore, the system performs with a PF equal to 1.

These good features of the grid current prove that the proposed algorithm is efficient to compensate the harmonic, reactive and unbalanced currents introduced in the grid by the unbalanced and nonlinear loads in any operating point of the PV system.

Furthermore, the DC bus voltage is also simulated and verified in the three modes. As shown in Fig.28, the DC voltage remains constant, equal to 840V in the three operating modes. This value is approximately equal to 2.8 times the line voltage.

**Table 3** THD and Magnitude values of the grid currents in the three modes

| | | $i_{ga}$ | $i_{gb}$ | $i_{gc}$ |
|---|---|---|---|---|
| **Mode 1** | THD (%) | 1.48 | 1.33 | 1.82 |
| | Mag (A) | 14.1 | 14.34 | 14.22 |
| **Mode 2** | THD (%) | 1.82 | 1.77 | 2.19 |
| | Mag (A) | 12.42 | 12.18 | 12.29 |
| **Mode 3** | THD (%) | 2.23 | 2.24 | 2.86 |
| | Mag (A) | 8.749 | 8.979 | 8.871 |

*4.5. Dynamic Response of the GCPVS*

In order to evaluate the dynamic response of the GCPVS with the proposed algorithm, the grid current is simulated under two different cases of solar irradiance variation represented in Fig.29. In the first case, the solar irradiance G is raised from 0W/m$^2$ to 1000W/m$^2$ at t= 0.4s, while in the second case, the solar irradiance G decreases from 1000W/m$^2$ to 200W/m$^2$ at t=0.6s. In these two cases, the simulated three-phase grid current response is illustrated in Fig.30, where a zoom on its dynamic behavior is highlighted at the moment of the solar irradiance change. As it can be noted, the three-phase grid current takes a short time to reach its steady-state, which is equal to 0.08s when the solar irradiance increases, and 0.06 s when the solar irradiance decreases. As a result, the GCPVS with the proposed algorithm presents a fast dynamic response.

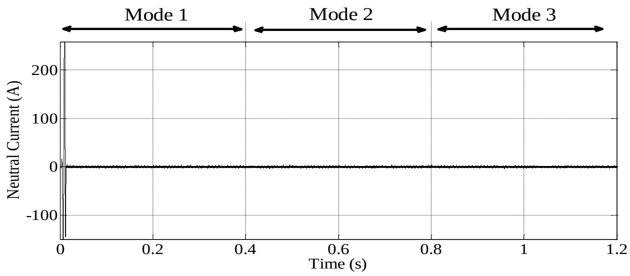


**Fig. 26.** Simulated neutral current

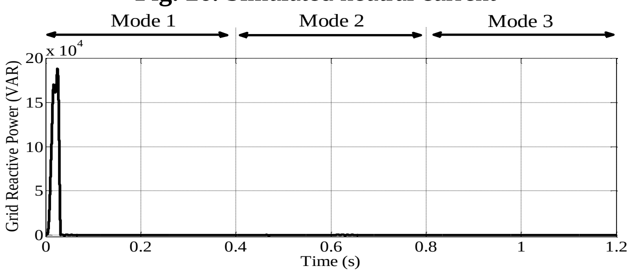


**Fig. 27.** Simulated reactive power of the grid

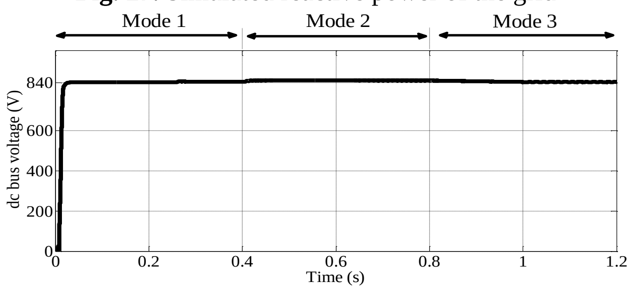


**Fig. 28.** The DC-bus voltage in the three operating modes

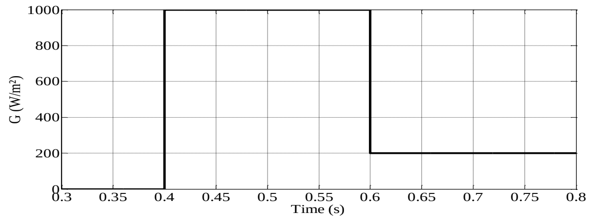


**Fig. 29.** Solar irradiance variation of the PV generator to study the dynamic response of the GCPVS

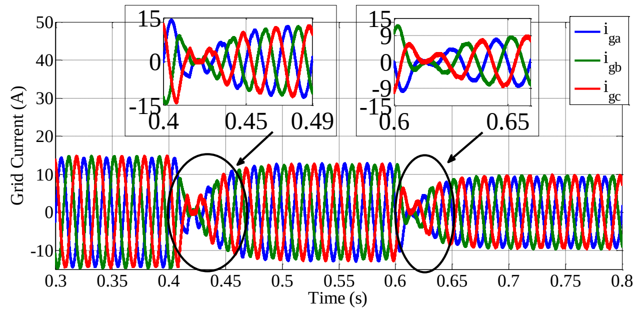


**Fig.30.** Dynamic response of the three-phase grid current with the proposed solar irradiation variation of Fig.32

*4.6. Comparison of the performance of the proposed algorithm and PQ based theory*

In order to evaluate the performance of the proposed algorithm, a comparison between the PQ theory and the proposed method is achieved under the same load conditions presented in Fig. 6.

Therefore, the THD index and the magnitude of the grid three currents obtained by the PQ method in the three modes are simulated. The frequency representation of the three grid currents $i_{ga}$, $i_{gb}$ and $i_{gc}$ are also illustrated in Figs 31, 32 and 33 for the three modes. As it is shown in Table 4, the THD of grid currents of the three phases in the three modes, obtained by the proposed method are better than the THD obtained by the PQ method. On the other hand, comparing to the magnitude values of the grid current presented in table 3, the proposed algorithm has demonstrated more satisfactory behaviour to rebalance the grid current. This is highlighted in Fig. 34 in which a zoom on the wave of the grid current in the three modes (Fig. 34 (b)) is presented. It can be noted that the amplitudes of the three grid currents have known a noticed difference in the three modes.

**Table 4** THD and Magnitude values of the grid currents in the three modes in case of PQ theory

| | | $i_{ga}$ | $i_{gb}$ | $i_{gc}$ |
|---|---|---|---|---|
| **Mode 1** | THD (%) | 1.96 | 2.44 | 2.2 |
| | Mag (A) | 14.08 | 14.46 | 14.17 |
| **Mode 2** | THD (%) | 2.26 | 2.01 | 2.73 |
| | Mag (A) | 12.49 | 12.11 | 12.34 |
| **Mode 3** | THD (%) | 2.91 | 3.44 | 3.13 |
| | Mag (A) | 8.749 | 9.158 | 8.868 |

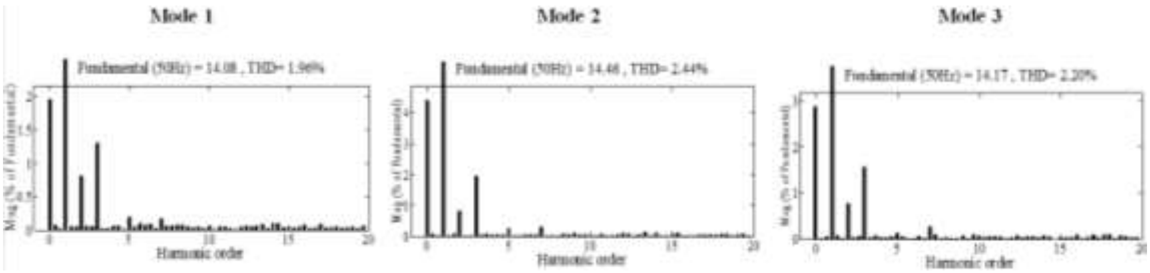


**Fig.31.** Frequency representation of the grid current of phase "a" in the three modes in case of PQ theory

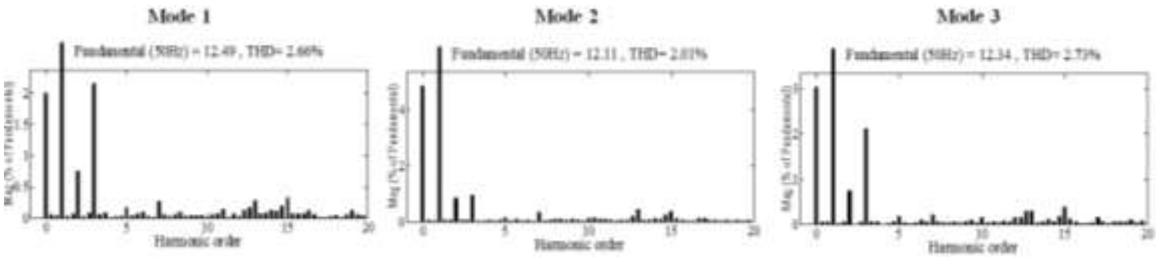


**Fig.32.** Frequency representation of the grid current of phase "b" in the three modes in case of PQ theory

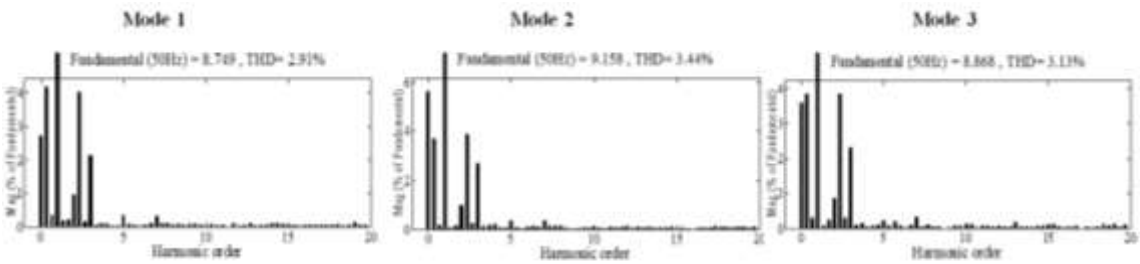


**Fig.33.** Frequency representation of the grid current of phase "c" in the three modes in case of PQ theory

However, the proposed algorithm for the extraction of the correct disturbing current permets to perfoms with a higher quality of the grid current at the PCC than in case of PQ theory.

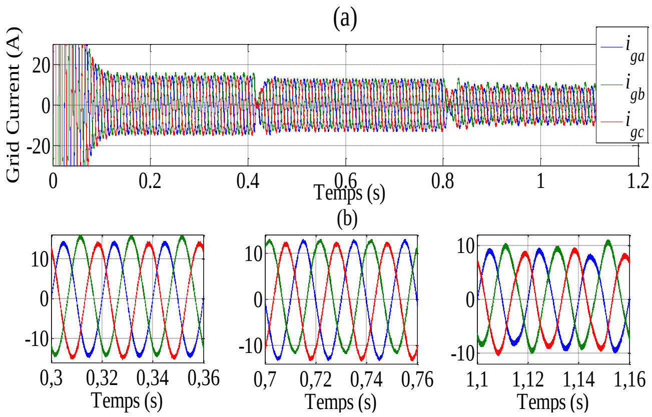


**Fig. 34.** Simulated three-phase grid current in the three operating modes in case of PQ theory(a) sample of 1.2 s (b) zoom on current wave in three modes

## 5. Conclusion

In this paper, the inverter of a three-phase grid connected photovoltaic system supplying unbalanced and nonlinear loads, was operated as a Shunt Active Power Filter (SAPF) in addition to its main role of power injection, in order to improve the quality of the grid current at the Point of Common Coupling (PCC). In this aim, in the PV inverter control strategy, a new algorithm is integrated to extract the disturbing current composed by the unbalanced, harmonic and reactive currents introduced by the connected loads. This technique is aimed to generate the reference compensating current of the current control loop in the control strategy of the PV inverter. According to the obtained results, it can be concluded that the PV inverter is able to inject the PV power and at the same time it compensates the unbalanced, harmonic and reactive currents under different levels of solar irradiance and temperature, to ensure a good quality of the grid current conform to the international standards

## Acknowledgements

This work was supported by the Tunisian Ministry of High Education and Scientific Research and the PHC-UTIQUE program (17/G 1131).

**References**

[1] A. Hintz, U. R. Prasanna, K. Rajashekara,"Comparative study of Three-phase Grid Connected Inverter Sharing Unbalanced Three-phase and/or Single-phase systems," Energy Conversion Congress and Exposition ECCE, 2015 IEEE, 20-24 September 2015.

[2] T. Demirdelen, R. I. Kayaalp, M. Tumay,"Simulation modelling and analysis of modular cascaded multilevel converter based shunt hybrid active power filter for large scale photovoltaic system interconnection, "Simulation Modelling Practice and Theory, vol. 71, pp. 27- 44, February 2017.

[3] Q. N. Trinh, H.H. Lee," An Enhanced Grid Current Compensator for Grid-Connected Distributed Generation Under Non Linear Loads and Grid Voltage Distortions," IEEE Transactions on Industrial Electronics, vol.61, no. 12 pp. 6528-6537, December 2014.

[4] Z. Liu, J. Liu, Y.Zhao," A unified Control Strategy for Three-Phase Inverter in Distributed Generation," IEEE Transactions on power electronics, vol.29, no.3, pp. 1176-1191 March 2014.

[5] M. Khatri, A. Kumar," Experimental Investigation of Harmonics in a Grid-Tied Soalr Photovoltaic System," International Journal of Renewable Energy Research, vol. 7, no. 2, pp. 901-907, 2017.

[6] R. M. Domingos, L. S. Xavier, A. F. Cupertino, H. A. Pereira," Current Control Strategy for Reactive and Harmonic Compensation with Dynamic Saturation," 24th IEEE ISIE'15, pp. 669 – 674, 3-5 June 2015.

[7] P.Thirumoorthi, N.Yadaiah ,"Design of current source hybrid power filter for harmonic current compensation," Simulation Modelling Practice and Theory, vol. 52, pp. 78-91, March 2015.

[8] T. H. Chen, C. H. Yang, T. Y. Hsieh, "Case Studies of the Impact of Voltage Imbalance on Power Distribution Systems and Equipment," Proceedings of the 8th WSEAS International Conference on Applied Computer and Applied Computational Science, pp. 461 – 465, 2009.

[9] N. Mesbahi, A. Ouari, D. Ould Abdeslamb, T. Djamah, A. Omeiri," Direct power control of shunt active filter using high selectivity filter (HSF) under distorted or unbalanced conditions," Electric Power Systems Research, vol. 108, pp. 113- 123, March 2014.

[10] T. Geury, S. Pinto, J. Gyselinck," Current source inverter-based photovoltaic system with enhanced active filtering functionalities," IET Power Electronics, vol. 8, no. 12, pp.1–9, May 2015.

[11] S. R. Arya, B. Singh, "Performance of DSTATCOM Using Leaky LMS Control Algorithm," IEEE Journal of Emerging and Selected Topics in Power Electronics, vol. 1, no. 2 ,pp 104-113, June 2013.

[12] B. Singh, S. Raj Arya, A. Chandra, K. Al-Haddad," Implementation of Adaptive Filter in Distribution Static Compensator," IEEE Transactions on Industry Applications, vol. 50, no. 5, pp 3026 – 3036, October 2014.

[13] Y. Bouzelata, H. Djeghloud, R. Chenni,"The Apllication of an Active Power Filter on a Phototovltaic Power Generation System,"Internatioanl Journal of Renewable Energy Research, vol. 2, no. 4, pp. 583-590, 2012.

[14] I. Aboudrar, S. El Hani, H. Mediouni, N. Bennis, A. Echchaachouai," Hybrid Algorithm and Active Filtering Dedicated to the Optimization and the Improvement of Photovoltic System connected to Grid Energy Quality, "Internatioanl Journal of Renewable Energy Research, vol. 7, no. 2, pp. 894-900, 2017.

[15] T. A. Youssef, A. T. Elsayed, A. Berzoy, O. A. Mohammed," Power Quality Enhancement for Nonlinear Unbalanced Loads through Improved Active Power Filter Control", IECON 2014 - 40th Annual Conference of the IEEE Industrial Electronics Society, pp. 5202 - 5207, 29 October - 1 November 2014.

[16] P. Panigrahi, B. Subudhi," Performance Enhancement of Shunt Active Power Filter using a Kalman Filter based H∞ Control Strategy," IEEE Transactions on Power Electronics, vol. 32, no.4, pp. 2622-2630, April 2017.

[17] L. Saribulut," A novel average filter based phase-locked loop for FACTS devices," Electric Power Systems Research, vol 136, pp. 289-297, March 2016.

[18] B. Singh, M. Kandpal, I. Hussain," Control of Grid Tied Smart PV-DSTATCOM System using an Adaptive Technique," IEEE Transactions on Smart Grid, vol. PP, no.99, pp. 1-7, December 2016.

[19] M. Badoni, A. Singh, B. Singh," Adaptive Neuro Fuzzy Inference System Least-Mean-Square Based Control Algorithm for DSTATCOM," IEEE Transactions on Industrial Informatics, vol. 12, no. 2, pp. 483-492, April 2016.

[20] M. Longhua, Jiangzi," Application of Adaptive Filtering in Harmonic Analysis and Detection," Transmission and Distribution Conference and Exhibition: Asia and Pacific, 2005 IEEE/PES, 14-18 August 2005.

[21] H. Li, Z. Wu, F. Liu, "A novel variable step-size adaptive harmonic detecting algorithm applied to active power filter," International Conference on Industrial Technology," 2006 IEEE/ICIT, 15-17 December, 2006.

[22] R. K. Agarwal, I. Hussain, B. Singh," LMF Based Control Algorithm for Single Stage Three-Phase Grid Integrated Solar PV System," IEEE Transactions on Sustainable Energy, vol. 7, no.4, pp 1379-1387, October 2016.

[23] R.K.Agarwal, I. Hussain, B. Singh," Implementation of LLMF Control Algorithm for Three-Phase Grid Tied SPV-DSTATCOM System," IEEE Transactions on

Industrial Electronics, vol. 6, no. 9, pp 7414-7424, September 2017.

[24] M. Srinivas, I. Hussain, B. Singh," Combined LMS-LMF Based Control Algorithm of DSTATCOM for Power Quality Enhancement in Distribution System," IEEE Transactions on Industrial Electronics, vol. 63, no. 7, pp 4160-4168, July 2016.

[25] M. Badoni, A. Singh," Variable Forgetting Factor Recursive Least Square Control Algorithm for DSTATCOM,"IEEE Transactions on Power Delivery, vol. 30, no.5, pp 2353-2361, October 2015.

[26] M. Qasim, V. Khadkikar," Application of Artificial Neural Networks for Shunt APF Control," IEEE Transactions on Industrial Informatics, vol. 10, no. 3, pp 1765 – 1774, August 2014.

[27] M. Badoni, A. Singh, B. Singh," Comparative Performance of Wiener Filter and Adaptive Least Mean Square Based Control for Power Quality Improvement," IEEE Transactions on Industrial Electronics, vol. 63, no. 5, pp 3028-3037, May 2016.

[28] G. Tsengenes, G Adamidis," A multi-function grid connected PV system with three level NPC inverter and voltage oriented control, " Solar Energy, vol 85 pp. 2595–2610 September 2011.

[29] S. Agarwal, M. Jamil," A Comparison of Photovoltaic Maximum Power Point Techniques," 2015 Annual IEEE India Conference (INDICON), pp. 1 – 6, 17-20 December. 2015.

[30] M. Tampubolon, I. Purnama, P. C. Chi, J. Y. Lin, Y. C. Hsieh, H. J. Chiu," A DSP-Based Differential Boost Inverter with Maximum Power Point Tracking," 9th International Conference on Power Electronics-ECCE Asia, pp. 309 – 314, 1-5 June 2015.

[31] X. Cao, S. Zhou, J. Li and S. Zhang," A DC Voltage Control Strategy for Active Power Filter," The Open Electrical & Electronic Engineering Journal, vol. 10, pp. 166- 180, July 2016.

[32] A. Hintz, U.R. Prasanna and K. Rajashekara," Comparative Study of Three-phase Grid Connected Inverter Sharing Unbalanced Three-phase and/or Single-phase systems," Energy Conversion Congress and Exposition ECCE, 2015 IEEE, 20-24 September 2015 .

[33] P. S. R Murty, Symmetrical Components, Power Systems Analysis, Edition 2, pp. 113-119, June 2017, Ch. 6.

[34] S. Golestan, M. Monfared, F. D. Freijedo, J. M. Guerrero," Performance Improvement of a Prefiltered Synchronous-Reference-Frame PLL by Using a PID-Type Loop Filter," IEEE TRANSACTIONS ON INDUSTRIAL ELECTRONICS, vol.61, no.7, pp. 3469-3479, July 2014.

[35] S. Chatterjee, S. Chatterjee," Simulation of Synchronous Reference Frame PLL based Grid Connected Inverter for Photovoltaic Application," ICPDEN 2015, 10-11 January 2015.